

Effect of Exciton-Phonon Coupling in the Calculated Optical Absorption of Carbon Nanotubes

Vasili Perebeinos, J. Tersoff, and Phaedon Avouris*

IBM Research Division, T. J. Watson Research Center, Yorktown Heights, New York 10598, USA

(Received 2 August 2004; published 19 January 2005)

We find that the optical properties of carbon nanotubes reflect remarkably strong effects of exciton-phonon coupling. Tight-binding calculations show that a significant fraction of the spectral weight of the absorption peak is transferred to a distinct exciton + phonon sideband, which is peaked at around 200 meV above the main absorption peak. This sideband provides a distinctive signature of the excitonic character of the optical transition. The exciton-phonon coupling is reflected in a dynamical structural distortion, which contributes a binding energy of up to 100 meV. The distortion is surprisingly long ranged, and is strongly dependent on chirality.

DOI: 10.1103/PhysRevLett.94.027402

PACS numbers: 78.67.Ch, 71.10.Li, 71.35.Cc

The optical properties of carbon nanotubes are currently the focus of intense experimental and theoretical attention [1–12], and even single nanotube electro-optical devices have been demonstrated [13–15]. Most of the experimental results have been discussed and analyzed in terms of interband transitions. In particular, nanotube band gaps were determined in this way. However, theoretical calculations of the optical spectra [10–12] suggest that the observed transitions correspond to exciton energies, not interband transitions. Moreover, the exciton binding energies are anomalously large in nanotubes [7,8,10–12], corresponding to a substantial fraction of the band gap, so the optical transition energy is quite different than the band gap.

If correct, these theoretical results require a reevaluation of our current picture of nanotube electronic structure. Device properties are particularly sensitive to the band gap because of the central role of tunneling in most nanotube transistors [16]. Thus a definitive test of the excitonic interpretation of optical transitions is needed. Fine structure in the optical data can provide a distinctive signature, facilitating comparison between different models to unambiguously verify the role of excitonic transitions. Recent photoconductivity excitation spectra [17,18] show sidebands at about 200 meV above to the main absorption peaks, suggesting the involvement of phonons. Fluorescence excitation spectroscopy also shows structure at the phonon energy, allowing more detailed analysis with finer energy resolution [19]. But while the interaction of single electrons with phonons has been studied extensively, we know of no studies of exciton-phonon interactions in nanotubes.

We therefore investigate theoretically the role of electron-phonon coupling in the optical spectra of nanotubes, including a comparison of between excitons and free-carrier transitions. We find surprisingly strong phonon effects in the excitonic spectra. Dynamical effects lead to the transfer of a significant fraction of the spectral weight from the exciton absorption peak (zero-phonon line) to a phonon sideband peaked at around 200 meV [Fig. 1(a) and Fig. 2(a) and 2(b)], consistent with the experimental observations. In contrast, our calculations for electron-

phonon interaction without excitonic binding [Fig. 2(c)] do not show a distinct phonon sideband. These results clearly suggest that the optical data must be interpreted in terms of excitonic transitions and do not provide a direct measure of the band gap.

We find that the fraction of the intensity transferred to the phonon sideband is inversely proportional to the nanotube diameter. The exciton-phonon binding energy is also unexpectedly high—about 60–100 meV. The associated lattice distortions exhibit an intriguing structure; they extend far beyond the exciton itself [11] and reverse sign for different nanotube chiralities [Fig. 1(b) and 1(c)]. The effect of the dielectric environment on the spectra is also discussed. (We treat individual nanotubes, as in fluorescence excitation spectroscopy. Nanotube bundles are less suitable for measuring detailed line shapes.)

In the absence of exciton-phonon coupling, emission or absorption of a photon involves an exciton of total wave vector q_ϕ corresponding to the photon momentum, hereafter approximated as $q_\phi = 0$. The exciton-phonon coupling mixes this exciton with phonons and with excitons of other q , such that the total exciton + phonon momentum is conserved. The finite- q exciton wave function can be found from the solution of the Bethe-Salpeter equation (BSE) [20] in the basis of a tight-binding Hamiltonian [21], analogous to the $q = 0$ case [11]:

$$|\Psi_q^S\rangle = \sum_k A_{kq}^S u_{k+q}^\dagger v_k |GS\rangle. \quad (1)$$

Here A_{kq}^S is the eigenvector of the S 's state of BSE solution; u_{k+q}^\dagger (v_k) creation (annihilation) of an electron in the conduction (valence) band acting on the ground state $|GS\rangle = \prod_k v_k^\dagger |\text{vac}\rangle$. The indices k and q each label both the continuous 1D wave vector along the tube axis and the discrete circumferential wave vector.

We model the electron-phonon interaction by the Su-Schrieffer-Heeger (SSH) model [22] with matrix element $t = t_0 - g\delta u$ dependent on the change of the nearest neighbor C-C distance (δu), where $t_0 = 3$ eV. We take the electron-phonon coupling constant to be $g = 5.3$ eV/Å as

predicted theoretically for a related molecular problem [23], consistent with fits to the Peierls gap in conjugated polymers [24].

After Fourier transformation, the intraband SSH Hamiltonian has the form

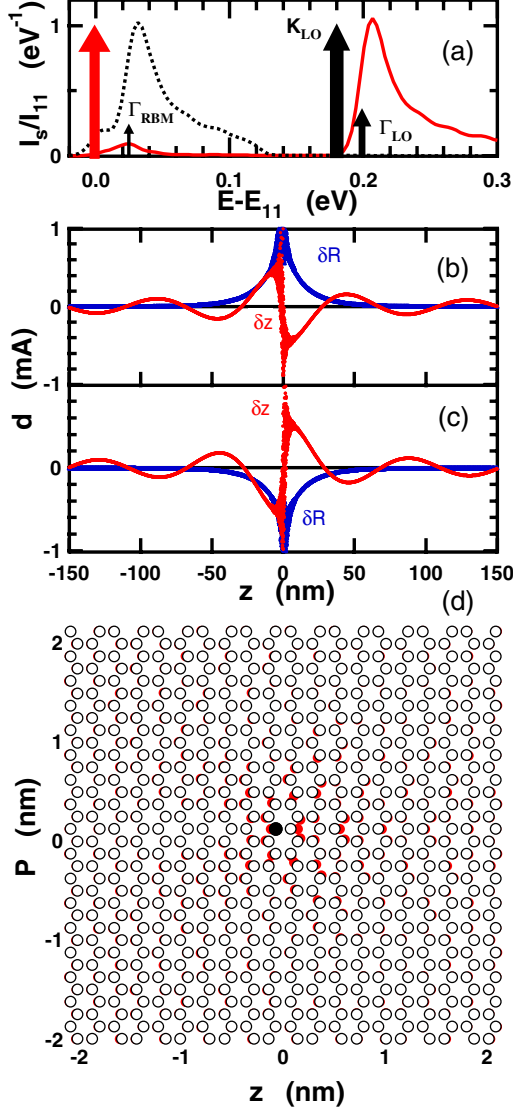


FIG. 1 (color online). (a) Absorption spectrum Eq. (4) for (17, 0) tube and $\epsilon = 2$ (solid red curve and red delta function). Dotted line shows electronic contribution to sideband energy (with 10 meV Gaussian broadening). Phonon contributions are quite narrow and are shown schematically as delta functions (height $\sim I^{1/2}$). (b) Long-range tail of the atomic displacements with respect to the hole position (at origin) for a (16, 0) tube: radial displacements (labeled δR , in blue), and displacements parallel to the axis (labeled δz , in red). (c) Same for (17, 0) tube. (d) Short-range azimuthal and axial distortions, shown on “unwrapped” carbon nanotube by displaying the displaced atom positions (red circles) together with undisplaced positions (white circles), with displacements magnified by a factor of 230 for visibility. Hole position is solid circle at center.

$$\mathcal{H}_{\text{el-ph}} = \sum_{kq\mu} M_{kq}^{\mu} (v_{k+q}^{\dagger} v_k - u_{k+q}^{\dagger} u_k) (a_{q\mu} + a_{-q\mu}^{\dagger}), \quad (2)$$

where $M_{kq}^{\mu} \propto gN^{-1/2}$ is momentum dependent electron-phonon coupling, $a_{-q\mu}^{\dagger}$ is a phonon creation operator with wave vector $-q$ and phonon band index $\mu = 1 \dots 6$, and N is the number of primitive unit cells, each containing two carbons. For the phonon spectrum we used a force-constant model similar to Saito *et al.* [25].

The electron-phonon Hamiltonian mixes the optically active $q = 0$ exciton with finite- q excitons in combination with phonons of wave vector $-q$:

$$\begin{aligned} \mathcal{H}_{\text{el-ph}} |\Psi_0^S\rangle &= - \sum_{S'q\mu} B_{q\mu}^{SS'} a_{-q\mu}^{\dagger} |\Psi_q^{S'}\rangle \\ B_{q\mu}^{SS'} &= \sum_k M_{kq}^{\mu} A_{kq}^{S'*} (A_{k,0}^S + A_{k+q,0}^S). \end{aligned} \quad (3)$$

Here the orthogonality relation of the BSE solution ($\sum_S A_{kq}^S A_{k'q}^{S*} = \delta_{kk'}$) has been used to derive exciton-phonon coupling amplitudes $B_{q\mu}^{SS'}$.

The wave function and the spectral line shape can be evaluated in second order perturbation theory for the lowest optically active exciton s :

$$\begin{aligned} |\tilde{\Psi}_0^s\rangle &\propto |\Psi_0^s\rangle + \sum_{qS'\mu} \frac{B_{q\mu}^{sS'}}{E_q^{S'} + \hbar\omega_{-q\mu} - E_0^s} a_{-q\mu}^{\dagger} |\Psi_q^{S'}\rangle \\ I(\omega) &\propto \delta(E_0^s - \hbar\omega) + \sum_{qS'\mu} \frac{|B_{q\mu}^{sS'}|^2}{(E_q^{S'} + \hbar\omega_{-q\mu} - E_0^s)^2} \\ &\quad \times \delta(E_q^{S'} + \hbar\omega_{-q\mu} - \hbar\omega). \end{aligned} \quad (4)$$

The calculated absorption spectrum Eq. (4) is shown in Fig. 1(a) (solid red curve) for a (17, 0) tube and $\epsilon = 2$, where ϵ is the dielectric constant of the embedding medium [11]. Because of exciton-phonon coupling, the main absorption peak loses 8% of its spectral weight to the sideband, which corresponds to the continuum of finite- q excitons plus phonon of wave vector $-q$. Most of the transferred spectral weight goes to the prominent sideband at about 210 meV above the zero-phonon line, with 4% of the spectral weight falling between 100 and 300 meV. The SSH Hamiltonian has little coupling to the low frequency modes and we find a much weaker replica at the radial breathing mode (RBM) frequency [about 20 meV for a (17, 0) tube].

To understand the spectrum in more detail, we decompose the sideband energy into contributions from phonon energy and exciton dispersion. Specifically, for each transition within 300 meV above the zero-phonon line, we project out the energy contribution from phonons vs electronic excitation (due to the admixture of finite- q excitons). The phonon contribution to the sideband exhibits three peaks Fig. 1(a), corresponding to the longitudinal optical (LO) phonon band edges at the K and Γ points of the graphene Brillouin zone, and the radial breathing

mode. The K phonon dominates. It has stronger coupling, and more importantly, it mixes exciton bands [26], allowing absorption by the “dark” (dipole forbidden) bands [11,27]. The energy difference between the sideband peak position and optical phonon frequency is due largely to the fact that the dark excitons that dominate the sideband are roughly 30 meV higher in energy than the optically active exciton, for the case shown in Fig. 1(a). (The broadening comes primarily from the “recoil energy,” i.e., the energy from finite exciton q .)

In the presence of an exciton, the nanotube distorts dynamically. While the electron remains within roughly 2 nm of the hole for the cases shown in Fig. 1, the structural distortions are far more long ranged. The distortions calculated using the wave function Eq. (1) are shown in Fig. 1(b) and 1(c) for (16, 0) and (17, 0) tubes, respectively, plotting the atomic displacements relative to the position of the hole. The breathing distortions decay exponentially away from the exciton, with a decay length of $\lambda_b = 13$ nm. We find that λ_b is proportional to the tube diameter. The sign of the breathing distortion depends on chirality indices (n, m): positive for $\text{mod}(n - m, 3) = 1$ and negative for $\text{mod}(n - m, 3) = 2$. From the sign of the exciton-phonon matrix elements, we expect a reversal of the signs of the breathing distortions for the second exciton. The displacements parallel to the tube axis decay far more slowly even than this, oscillating with a wave vector $\lambda_z \approx 80$ nm, which appears to be insensitive to the tube diameter. The short-range distortions near the exciton are shown in Fig. 1(d).

The spectra for higher-energy excitons ($E_0^S > E_0^s$) cannot be obtained from Eq. (4) because the denominator $E_q^{S'} + \hbar\omega_{-q\mu} - E_0^S$ can be arbitrarily close to zero and the perturbation theory breaks down. Toyozawa showed [28] that an exact solution for the absorption spectra has a form similar to the perturbation theory expression, with an energy dependent lifetime and polaronic shift in the energy denominator. We approximate Toyozawa’s solution by evaluating the lifetime broadening in the random phase approximation (RPA):

$$I(\omega) = \sum_S \frac{f_S}{\pi} \frac{\Gamma_S(\omega)}{(\hbar\omega - E_0^S)^2 + \Gamma_S(\omega)^2}$$

$$\Gamma_S(\omega) = \pi \sum_{S'q\mu} |B_{q\mu}^{SS'}|^2 \delta(\hbar\omega - E_q^{S'} - \hbar\omega_{-q\mu}), \quad (5)$$

where f_S is the oscillator strength of the S exciton [11]. We checked that the Toyozawa solution obtained with a self consistent Born approximation neglecting the k dependence of the self energy $\Sigma_S(E) = \Delta_S(E) + \Gamma_S(E)$ does not change the RPA result Eq. (5). If $\hbar\omega = E_0^S$ in Eq. (5) then $\Gamma_S(E_0^S)/\hbar$ equals half of the reciprocal lifetime of S exciton due to the scattering by phonons. The binding energy shift for the S exciton in RPA approximation is:

$$\delta E_S = \sum_{S'q\mu} |B_{q\mu}^{SS'}|^2 \mathcal{P}(E_0^S - E_q^{S'} - \hbar\omega_{-q\mu})^{-1}, \quad (6)$$

where \mathcal{P} denotes the principle part.

The absorption spectra calculated with and without exciton-phonon coupling are shown in Fig. 2 for the tube embedded in dielectric $\epsilon = 2, 4$, and for the free electron-hole pair absorption (equivalent to the limit $\epsilon \rightarrow \infty$). In the absence of exciton-phonon interactions there are two strong exciton absorption peaks, each followed by the corresponding continuum of intraband absorption [11]. The first exciton has zero width in this approximation and is shown by a vertical arrow in Fig. 2(a) and 2(b). Both exciton lines show a distinct phonon sideband about 200 meV above the main absorption line. [For $\epsilon = 4$ the exciton binding energy is about 0.2 eV, so the band-to-band absorption (dotted line) also contributes to the sideband intensity in Fig. 2(b).] In contrast, there is no distinct phonon peak associated with band-to-band absorption [Fig. 2(c)]. Thus the phonon peak provides a clear signature of whether or not the absorption is excitonic in nature.

The second exciton can decay into free electron-hole pairs of the first band via Coulomb interaction or by emitting a phonon, giving rise to a finite lifetime of the second exciton resonance. The electronic and phonon contribu-

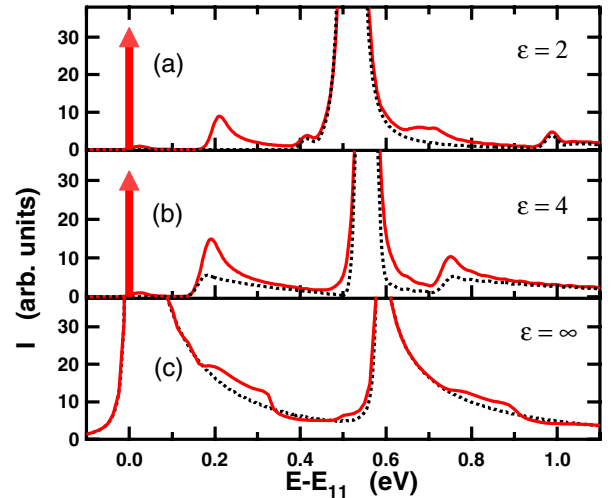


FIG. 2 (color online). Absorption spectra in (17, 0) tube calculated with and without electron-phonon couplings (solid red and dashed black curves, respectively) for (a) $\epsilon = 2$, (b) $\epsilon = 4$, (c) $\epsilon \rightarrow \infty$. The zero of energy here corresponds to the onset of the first optically active exciton, which has zero width and is shown by the vertical arrows. The onset of continuum (band gap) transitions is at 0.48 eV, 0.19 eV, and 0 in (a), (b), and (c), respectively. The width of the second exciton is finite due to: (1) coupling with the first band electron-hole continuum to give lifetimes of $\tau_{ee} = 10$ and 15 fs for $\epsilon = 2$ and 4, respectively; and (2) coupling with phonons to give $\tau_{ph} = 90$ and 33 fs for $\epsilon = 2$ and 4, respectively. Delta functions in Eq. (5) were Gaussian broadened with width of 20 meV, except in (c) we use 6.5 meV to emphasize that the width of the continuum peak is intrinsic.

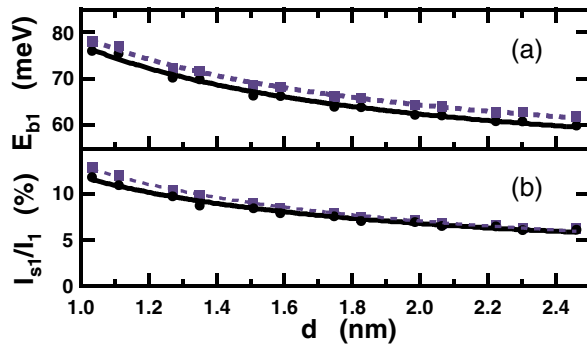


FIG. 3 (color online). (a) The phonon binding energy and (b) fraction of the spectral weight transferred to the exciton + phonon sideband for the first exciton in zigzag tubes versus tube diameter for $\epsilon = 2$ (black circles) and for $\epsilon = 4$ (blue squares), respectively. The curves (black solid for $\epsilon = 2$ and blue dashed for $\epsilon = 4$) are fits $A_{b,I} + B_{b,I}/d$, where $A_b = 47$ (meV), $B_b = 30$ (meV nm) and $A_I = 1.7$ (%), $B_I = 10$ (% nm) for $\epsilon = 2$.

tions are given in the figure caption for a (17, 0) tube for two values of ϵ . The actual value of the lifetime, as well as other details of the spectrum, are very sensitive to the lineup of the resonance peak position with the onset of the first band continuum, and thus are also sensitive to the tube radius and dielectric environment. Therefore experimental measurements of the first exciton are easier to compare with theory.

The total exciton-phonon binding energy calculated from Eq. (6) has the largest contribution from the coupling to the higher-energy states, which have smaller optical spectral weight due to the energy denominator in Eq. (5). The dependence of the binding energy on the diameter d is shown in Fig. 3(a), along with a phenomenological fit, for the first exciton in different zigzag tubes, for $\epsilon = 2$ and 4. The second exciton binding energy is always larger than the first exciton—by 15%–30%—due to the larger effective mass of the former. The fraction of the spectral weight transfer for the first exciton Eq. (4) is shown on Fig. 3(b), along with a fit for the same values of ϵ .

In conclusion, we calculate exciton-phonon effects in the absorption spectra of carbon nanotubes, predicting a significant spectral weight transfer from the main (excitonic) absorption peak to a phonon sideband at around 200 meV above the zero-phonon line, for both the first and second excitons. Comparable structure is seen in recent experiments [17–19]. In contrast, for band-to-band transitions we find that there is no distinct sideband; instead, the phonon structure represents only a slight perturbation of the spectrum. We therefore believe that the phonon sideband provides direct experimental evidence that the optical transition is excitonic in nature and cannot be used as a direct measure of the band gap.

- [1] Z. M. Li, Z. K. Tang, H. J. Liu, N. Wang, C. T. Chan, R. Saito, S. Okada, G. D. Li, J. S. Chen, N. Nagasawa, and S. Tsuda, *Phys. Rev. Lett.* **87**, 127401 (2003).
- [2] M. J. O'Connell, S. M. Bachilo, C. B. Huffman, V. C. Moore, M. S. Strano, E. H. Haroz, K. L. Rialon, P. J. Boul, W. H. Noon, C. Kittrell, J. Ma, R. H. Hauge, R. B. Weisman, and R. E. Smalley, *Science* **297**, 593 (2002).
- [3] S. M. Bachilo, M. S. Strano, C. Kittrell, R. H. Hauge, R. E. Smalley, and R. B. Weisman, *Science* **298**, 2361 (2002).
- [4] A. Hagen and T. Hertel, *Nano Lett.* **3**, 383 (2003).
- [5] S. Lebedkin, F. Hennrich, T. Skipa, and M. M. Kappes, *J. Phys. Chem. B* **107**, 1949 (2003).
- [6] J. Lefebvre, Y. Homma, and P. Finnie, *Phys. Rev. Lett.* **90**, 217401 (2003).
- [7] T. Ando, *J. Phys. Soc. Jpn.* **66**, 1066 (1997).
- [8] T. G. Pedersen, *Phys. Rev. B* **67**, 073401 (2003).
- [9] C. L. Kane and E. J. Mele, *Phys. Rev. Lett.* **90**, 207401 (2003).
- [10] C. D. Spataru, S. Ismail-Beigi, L. X. Benedict, and S. G. Louie, *Phys. Rev. Lett.* **92**, 077402 (2004); *Appl. Phys. A* **78**, 1129 (2004).
- [11] V. Perebeinos, J. Tersoff, and Ph. Avouris, *Phys. Rev. Lett.* **92**, 257402 (2004).
- [12] E. Chang, G. Bussi, A. Ruini, and E. Molinari, *Phys. Rev. Lett.* **92**, 196401 (2004).
- [13] J. A. Misewich, R. Martel, Ph. Avouris, J. C. Tsang, S. Heinze, and J. Tersoff, *Science* **300**, 783 (2003).
- [14] M. Freitag, Y. Martin, J. A. Misewich, R. Martel, and Ph. Avouris, *Nano Lett.* **3**, 1067 (2003).
- [15] M. Freitag, J. Chen, J. Tersoff, J. C. Tsang, Q. Fu, J. Liu, and Ph. Avouris, *Phys. Rev. Lett.* **93**, 076803 (2004).
- [16] S. Heinze, J. Tersoff, R. Martel, V. Derycke, J. Appenzeller, and Ph. Avouris, *Phys. Rev. Lett.* **89**, 106801 (2002); S. Heinze, M. Radosavljević, J. Tersoff, and Ph. Avouris, *Phys. Rev. B* **68**, 235418 (2003).
- [17] Ph. Avouris, *MRS Bull.* **29**, 403 (2004).
- [18] M. Freitag *et al.* (to be published).
- [19] S. G. Chou, F. Plentz Filho, J. Jiang, R. Saito, D. Nezich, H. B. Ribeiro, A. Jorio, M. A. Pimenta, Ge. G. Samsonidze, A. P. Santos, M. Zheng, G. B. Onoa, E. D. Semke, G. Dresselhaus, and M. S. Dresselhaus (unpublished).
- [20] M. Rohlfing and S. G. Louie, *Phys. Rev. B* **62**, 4927 (2000).
- [21] R. Saito and H. Kataura, in *Carbon Nanotubes: Synthesis, Structure, Properties and Application*, edited by M. S. Dresselhaus, G. Dresselhaus, and Ph. Avouris (Springer-Verlag, Heidelberg 2001), Vol. 80.
- [22] W. P. Su, J. R. Schrieffer, and A. J. Heeger, *Phys. Rev. Lett.* **42**, 1698 (1979); *Phys. Rev. B* **22**, 2099 (1980).
- [23] V. Perebeinos, P. B. Allen, and M. Pederson, *cond-mat/0208051*.
- [24] R. Fincher *et al.*, *Solid State Commun.* **27**, 489 (1978).
- [25] R. Saito *et al.*, *Phys. Rev. B* **57**, 4145 (1998).
- [26] V. Perebeinos, J. Tersoff, and Ph. Avouris, *cond-mat/0411021*.
- [27] H. Zhao and S. Mazumdar, *Phys. Rev. Lett.* **93**, 157402 (2004).
- [28] Y. Toyozawa, *Prog. Theor. Phys.* **20**, 53 (1958); *J. Phys. Chem. Solids* **25**, 59 (1964).

*Electronic address: avouris@us.ibm.com